Sun *et al. Energy Mater* 2024;4:400047
DOI: 10.20517/energymater.2024.03

Energy Materials

Article

Open Access

Check for updates

Guiding lithium growth direction by Au coated separator for improving lithium metal anode

Zhouting Sun[1,2,#], Qihang Zhang[1,#], Zhenyu Wang[1], Yifei Chen[1], Kaiming Wang[1,3], Fei Shen[1,*], Juchen Guo[4], Xiaogang Han[1,*]

[1]State Key Laboratory of Electrical Insulation and Power Equipment, School of Electrical Engineering, Xi'an Jiaotong University, Xi'an 710049, Shaanxi, China.
[2]Huaneng Clean Energy Research Institute, China Huaneng Group, Beijing 102200, China.
[3]School of Future Technology, Xi'an Jiaotong University, Xi'an 710049, Shaanxi, China.
[4]Department of Chemical and Environmental Engineering, Materials Science and Engineering Program, University of California, Riverside, CA 92521, USA.
[#]Authors contributed equally.

***Correspondence to:** Dr. Fei Shen, State Key Laboratory of Electrical Insulation and Power Equipment, School of Electrical Engineering, Xi'an Jiaotong University, Xi'an 710049, Shaanxi, China. E-mail: feishen@xjtu.edu.cn; Prof. Xiaogang Han, State Key Laboratory of Electrical Insulation and Power Equipment, School of Electrical Engineering, Xi'an Jiaotong University, Xi'an 710049, Shaanxi, China. E-mail: xiaogang.han@xjtu.edu.cn

How to cite this article: Sun Z, Zhang Q, Wang Z, Chen Y, Wang K, Shen F, Guo J, Han X. Guiding lithium growth direction by Au coated separator for improving lithium metal anode. *Energy Mater* 2024;4:400047. https://dx.doi.org/10.20517/energymater.2024.03

Received: 4 Jan 2024 **First Decision:** 20 Mar 2024 **Revised:** 17 Apr 2024 **Accepted:** 6 May 2024 **Published:** 16 May 2024

Academic Editors: Jiaqi Huang, Jinqiang Zhang **Copy Editor:** Fangyuan Liu **Production Editor:** Fangyuan Liu

Abstract

Lithium metal is the most promising anode for next-generation batteries due to its highest theoretical capacity and lowest electrochemical potential. However, its dendritic growth hinders its practical use due to the consequent poor reversibility, potential short-circuit, and safety concerns. Suppressing lithium dendrite is difficult since dendritic growth is thermodynamically and kinetically favorable. Herein, we guide lithium to uniformly deposit along the opposite direction to normal by a nanolayer Au coating on a commercial polypropylene separator. It prevents lithium dendrites from piercing the separator, instead of inhibiting dendrites growth only. Au is lithiophilic, and lithium is calculated to be more attracted to Au and is confirmed to uniformly deposit on Au at the separator side rather than on the current collector side. Furthermore, Au also regulates the morphology of deposited lithium from a mossy state to a bulky state. In this work, the symmetric cell with the designed structure achieves excellent electrochemical performances of a long-life cycle over 2,000 h at 1 C for 1 mA h cm^{-2}. Pairing with $LiFePO_4$ cathode as a full cell, lithium metal anode with Au-modified polypropylene separator exhibits extraordinary performance with a high Coulombic efficiency of 99.23% over 800 cycles at 1 C.

Keywords: Lithium metal anode, lithium dendrite, growth direction regulation, safety

INTRODUCTION

With the increasing demands for chargeable devices, including portable devices and large-scale grid, batteries with high-energy density (over 500 W h kg^{-1}) are urgently needed. Lithium metal is expected to be the ideal anode for the next-generation high-performance batteries, with its light-weight (0.53 g cm^{-3}), ultrahigh specific capacity (theoretically 3,860 mA h g^{-1}), and the lowest electrochemical potential (-3.04 V *vs.* standard hydrogen electrode). However, low Coulombic efficiency (CE), rapid capacity decay, and safety concerns obstruct its practical use. The main issues are its dendritic growth and infinite volume expansion[1].

Naturally, lithium protrusions are usually generated during lithium deposition due to uneven electric field and ion concentration. They are in a higher electrical field to attract more Li^+ flux. The continuous preferential growth on tips leads to the growth of irregular lithium, as dendrites. Once lithium dendrites grow enough, they will pierce the separator and reach the other electrode to cause short-circuit, posing safety hazard.

Consecutive strategies have been proposed to weaken and eliminate lithium dendritic growth[1-8]. Conductive scaffold with a high surface area is a common strategy to reduce the local current density, which can also accommodate the deposited lithium and buffer large volume change of anode during cycling. The scaffold materials are usually carbon and Cu[1,9-11]. However, lithium deposition is usually hindered by the poor affinity of Cu or carbon with lithium due to high nucleation barrier. Because an extensive electric field is on the 3D scaffold surface, and the local current density and Li^+ ion flux continuously decrease inside it[12], lithium mainly deposits on the surface rather than inside the scaffold, which cannot fully use the structure. Therefore, lithiophilic promoters, such as Si, Au[13], Ag[14], and ZnO[15-19], have been used to regulate lithium deposition. The modified scaffolds provide both an even distribution of electric fields and uniformly distributed nucleation sites as 3D hosts. Additionally, compressive stress is ubiquitous and cannot be easily relieved. It has been considered to relate to lithium plating morphology, making lithium dendrites emerge anywhere on the substrate surface[20]. When lithium grows in a common direction, the localization stress concentration would assist dendrite growth in piercing the separator[21,22]. This means that managing the compressive stress will greatly alleviate the dendrite growth.

Safety concerns usually come from inevitable dendrites piercing the soft separator. Natural solid electrolyte interphases (SEI) crack and regenerate during cycles, and lithium prefers to grow from exposed sites underlying cracked SEI, which intensifies its dendritic morphology growth. LiF coating[4], supramolecular polymer[7], inorganics[23], and alloy with lithium metal[24] are usually used to form an ultra-strong SEI. Separators are key components of rechargeable batteries; Al_2O_3[25], SiO_2[26], and a water-borne nanosized molecular sieve[27] were coated on the separator to enhance mechanical strength so that dendrites can be suppressed. Surface grafting technology[28-30] enhances the wettability and heat resistance of separators to improve battery performance. Solid-state electrolytes are also believed to prevent lithium dendrite growth from the current collector to the opposite electrode due to their superior mechanical strength[8,31-33].

All these strategies above focus on eliminating lithium dendrites by stopping their growth. In these strategies, lithium deposits in a common direction from the current collector side to the separator side. Herein, we design a nanolayer Au-modified polypropylene separator (AuPP), guiding uniform lithium deposition by lithiophilic Au and regulating the deposition direction. In this design, lithium grows from AuPP to the Cu side, along an opposite direction unlike common strategies, which reduces the probability of piercing the separator. Lithium ions prefer to deposit on the lithiophilic Au layer rather than on the

lithiophobic Cu foil. Besides, lithiophilic promoters, Au, provide homogeneous lithium nucleation sites. Additionally, the uneven compressive stress from lithium plating can be relieved by the nether soft AuPP, which could effectively mitigate lithium dendrite growth by reducing its driving force. In this work, the synergistic effects of regulated lithium deposition direction and uniformly deposited lithium morphology by the Au layer, along with relieved residual stress by soft AuPP, contribute to excellent electrochemical performances of lithium metal anodes.

EXPERIMENTAL

Preparation of separator with Au nanolayer.

The commercial Polypropylene (PP) (Celgard, USA) was used as a substrate. Au nanolayer was deposited on the substrate by a Turbomolecular pumped coater (Q150T Plus, UK) at 20 mA for 120 s.

Thickness measurement of Au nanolayer

A flat silicon wafer was used to substitute the PP as a substrate for Au to sputter on at the same condition as the preparation of AuPP. The Tape covers half of the silicon wafer to make a step between the wafer and sputtered Au. This thickness was measured by an atomic force microscope (AFM) (INNOVA, US).

Characterization

The scanning electron microscope (SEM) images were characterized using a Phenom ProX microscope (US), and the energy dispersive X-ray analysis (EDS) mappings were tested by an energy dispersive spectrometer (Phenom ProX microscope, US). X-ray diffraction (XRD) data were obtained from Bruker AXS diffractometer (UK). Optical video was characterized by a digital microscope (Dino-Lite Edge, China).

Electrochemical measurements

All coin cells were assembled using CR2025 coin-type cells in an Ar-filled glove box with the atmospheric condition of < 0.1 ppm oxygen and < 0.01 ppm H_2O. PP was employed as the separator. All electrochemical tests were carried out in an electrolyte of 1 M lithium bis (trifluoromethanesulfonyl) imide (LiTFSI, 1.0 mol L^{-1}) in 1,3-dioxolane (DOL)/1,2-dimethoxyethane (DME) (v/v = 1:1) with 2 wt% of lithium nitrates as additive. 60 μL of electrolyte was used in each coin cell.

To study CE, coin cells were assembled with PP or AuPP as the separator, Cu as the working electrode, and lithium foil as the counter electrode. Au is placed facing the Cu side. Cells were cycled at various currents with a charging cutoff voltage of 1 V. For the symmetric cells, lithium foils were placed on two sides of PP or AuPP. Full cells were assembled with $LiFePO_4$ cathodes (4.2 mg cm^{-2}). An amount of 1 mA h cm^{-2} lithium has been deposited on the AuPP and PP at 1 mA cm^{-2} as anodes in advance, corresponding with the negative/positive capacity ratio (N/P) ratio of 1.4. The cells were cycled between 2.5 and 4.0 V *vs.* Li^+/Li. The current density here is 170 mA g^{-1} for 1 C.

Calculation method

All our calculations were performed using the plane-wave Vienna Ab initio Simulation Package (VASP)[34,35]. A projector augmented-wave (PAW) pseudopotential method was applied to describe interactions between core and valence electrons[36]. A kinetic energy cutoff of 500 eV and a Γ-centered 2 × 2 × 1 k-point mesh were adopted. These parameters are necessary for convergence of the total energy to within 10^{-5} eV per atom and force less than 0.01 eV/Å per atom. The PBEsol functional, a version of Perdew-Burke-Ernzerh (PBE) functional revised for solids, was used for geometry optimization[37]. To investigate the interaction between Li and Cu, Au surfaces, and surface diffusion of Li, 4 × 4 Cu(111) and 4 × 4 Au(111) supercells were built, of which large sizes necessitate the vanishment of image charge interaction of adsorbed Li atoms. Each asymmetric surface slab was built with a vacuum region of 18 Å,

enough to ensure vanishing wave function overlap across the vacuum region. Among all slabs, the bottom two layers of atoms are fixed during the relaxation. The binding energy E_b denoted as

$$E_b = E_{sub} + \mu_{Li} - E_{sub+Li}$$

is calculated in terms of the total energy of the substrate with an adsorbed Li (E_{sub+Li}) and the bare substrate (E_{sub}), and chemical potential of Li (μ_{Li}), which is taken from the total energy of lithium metal per atom. The climbing image nudged elastic band (CI-NEB) method is applied to compute diffusion barriers[38].

RESULTS AND DISCUSSION

The morphology of deposited lithium on the AuPP and Cu is schematically illustrated in Figure 1A and B. A nanolayer Au is sputtered on the PP separator. In this design, lithium deposits on Cu and grows towards the separator without AuPP, while with AuPP, lithium deposits on AuPP and uniformly grows in the opposite direction to the current collector side. To confirm this hypothesis, in-situ optical observation was conducted, as shown in Supplementary Video 1 and Figure 1C. Cu, AuPP, and lithium foil have been stacked tightly and immersed in the electrolyte to simulate the real cell condition. A current density of 100 μA cm^{-2} has been applied. From Figure 1C, initially, Au and Cu tightly contact to provide an electronic path to Au on the separator. After 15 min, lithium is deposited on AuPP instead of Cu, despite their proximity. This suggests a preference for deposition on Au rather than Cu. After 20 min, the thickness of deposited lithium increases, meaning continued growth on the early deposits on the AuPP. To explain this phenomenon, binding energy was calculated to measure the affinity of lithium with substrates because lithium prefers to deposit on the substrate with higher binding energy. The calculated binding energy of lithium on Au (111) is 3.056 eV, higher than that on Cu (111) of 2.500 eV [Figure 1D], manifesting that Au is more lithiophilic for lithium to deposit on. This result is consistent with the lithium deposition phenomenon in the optical observation. Contact angles are tested to demonstrate the lithiophilic properties of two substrates. When the molten lithium drops on Cu, the contact angle is 136°, while it is only 12° on Au [Figure 1E and F]. This means that Cu is lithophobic and molten lithium readily wet Au, verifying that lithium is more favorable to Au. Additionally, because molten lithium finds it difficult to wet Cu, lithium droplets can easily move on the Cu surface. It makes the deposited lithium on Cu very messy, which is a hotbed for lithium dendrites [Figure 1A], while lithium can deposit on Au regularly due to the greater wettability [Figure 1B].

From the SEM images of the morphology of pristine PP and AuPP, Au is sputtered conformally on the PP membrane [Supplementary Figure 1A and B]. The typical stretched pore-forming structure of the PP separator is maintained, and its permeability will not be affected. Sputtering is an industrial method, so sputtering Au on the PP could be easily achieved on a large scale, as shown in the inset in Supplementary Figure 1B. From the EDS mapping images, the sputtered Au is uniformly distributed on the PP surface [Supplementary Figure 1C and D] The thickness of the sputtered Au is measured as 13.4 nm by the AFM [Supplementary Figure 2], which will not significantly influence the energy density of the battery.

To analyze the lithium nucleation and deposition behavior, a small amount of lithium of 0.2 mA h cm^{-2} at 1 mA cm^{-2} is deposited on the substrate, demonstrating the early stage of lithium nucleation distribution. Before lithium deposition, the Cu [Figure 2A] and AuPP [Figure 2B] surfaces are clean. On the Cu surface, deposited lithium forms clusters of islands, leaving the underlying Cu bare [Figure 2C], whereas on the AuPP surface, lithium is uniformly dispersed [Figure 2D]. When the lithium amount increases to 0.5 mA h cm^{-2}, the difference of lithium morphology on the two substrates becomes more significant [Figure 2E and F]. To investigate the effect of Au on lithium growth, a low current density of 10 μA cm^{-2} is

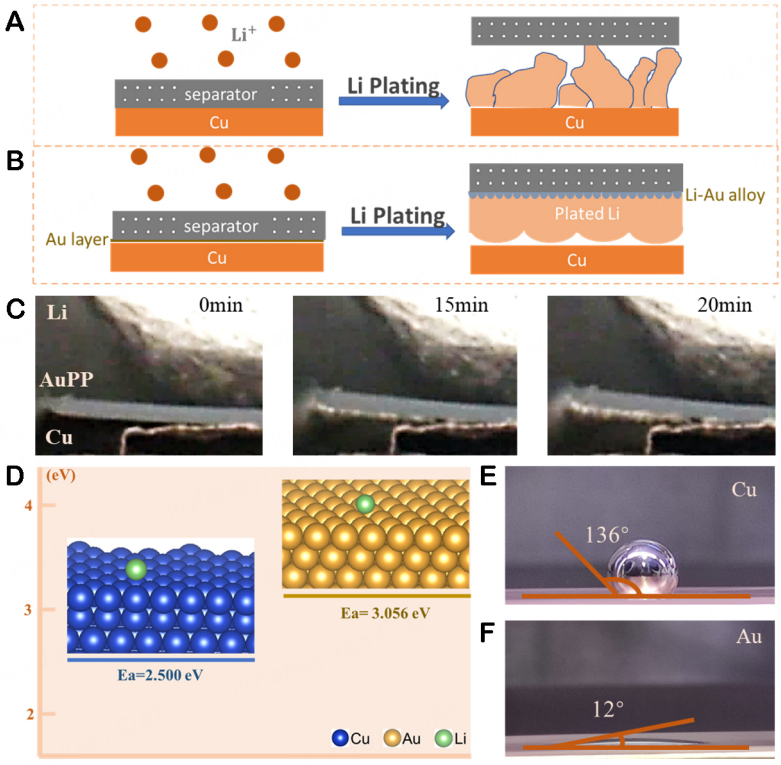

Figure 1. Schematic illustration of lithium depositing on (A) Cu and (B) AuPP. (C) Optical images of cross-section view of the simulated cell after lithium depositing for 0, 15 and 20 min. (D) Calculated binding energy of a lithium ion with Cu and Au. The contact angles of molten lithium with (E) Cu and (F) Au.

used to sluggishly deposit lithium [Supplementary Figure 3], eliminating mass transport influence. Supplementary Figure 3A and B shows the voltage profiles of lithium deposition on the Au and Cu. A significant voltage dip appears on Cu initially, which is absent on Au. The lowest and final stable voltage difference is termed overpotential, corresponding to the heterogeneous nucleation barrier. This overpotential is almost 0 mV on Au, meaning little nucleation barrier for lithium, while it is 20 mV on Cu. The higher nucleation overpotential on Cu is due to the large thermodynamic mismatch and interfacial energy between Li and Cu[39]. Flat voltage plateaus of 200 and 80 mV on Au correspond to alloying processes of Li_xAu. When the cutoff voltage is set as 0.001 V, there is no visible lithium on the AuPP surface and the element Au is uniformly distributed [Supplementary Figure 4], coinciding with the existence of alloys. To verify the final alloy phase under electrochemical depositing, we sputter Au on the Cu substrate with the same conditions but further time to make it measurable under XRD. From Supplementary Figure 5, after alloying, Au peaks disappear and $AuLi_3$ peaks emerge, indicating the final alloy as $AuLi_3$. This alloy layer is also the reason for eliminating the nucleation barrier for lithium depositing on the AuPP. These results indicate that the sputtered Au on PP helps eliminate the nucleation barrier and induce uniform nucleation sites, leading to a uniform and smooth growth of lithium.

From cross-section view of deposited lithium on Cu in Figure 2G, lithium grows from Cu foil but in wide size distribution, implying different growth times at these lithium sites. From the cross-section view of the AuPP [Figure 2H], lithium grows from the Au instead of the Cu current collector and tightly connects. The element mapping of lithium on the AuPP is conducted to clarify the lithium distribution [Supplementary Figure 6A]. Three distinguishing components are identified: the PP, Au layer, and deposited lithium. The upper part of element carbon (C) mapping coincides with the PP position, and the

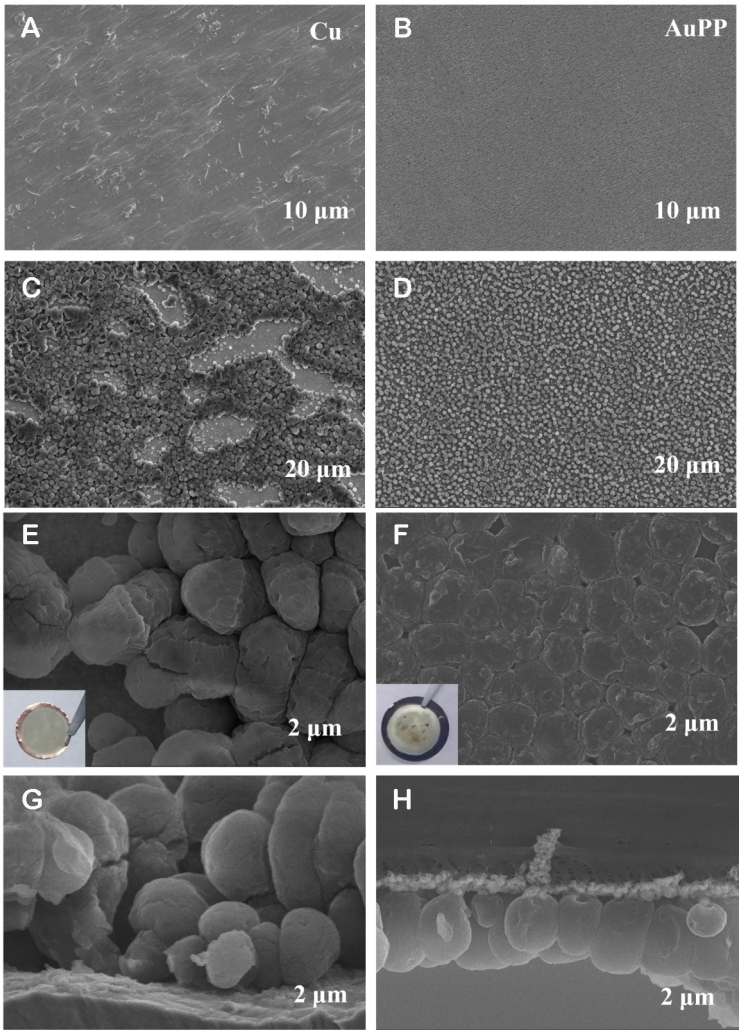

Figure 2. Nucleation and growth behavior of Li depositing on the Cu and AuPP. Top view of deposited lithium of 0, 0.2 and 0.5 mA h cm^{-2} at 1 mA cm^{-2} on the (A, C, E) Cu and (B, D, F) AuPP. Insets are digital photos of deposited lithium on two substrates. Cross-section view of deposited lithium on the (G) Cu and (H) AuPP with a capacity of 0.5 mA h cm^{-2} at 1 mA cm^{-2}.

lower part matches the lithium [Supplementary Figure 6B]. A bright Au band aligns with the Au layer position on the cross-section of AuPP [Supplementary Figure 6C]. The element mapping of the oxygen (O) corresponds to the deposited lithium distribution because of the lithium oxidation from the sample preparation process. The root of the deposited lithium is from the Au layer [Supplementary Figure 6D]. These results align with the calculated binding energies, indicating lithium preferentially nucleates on the Au rather than the Cu and grows from the AuPP to the Cu current collector.

The voltage profile of symmetric Li|Li cells with and without AuPP of a capacity of 1 mA h cm^{-2} at 1 mA cm^{-2}, as shown in Figure 3A, evaluates the electrochemical performances. The voltage platform of the symmetric cell with PP keeps oscillating in the early stage but tends to gradually expand and eventually lose control. In comparison, the cell with AuPP displays a very stable voltage hysteresis and long-term cycling stability. From the voltage profiles of the 50th, 500th and 1,000th cycles [Supplementary Figure 7], the hysteresis of the cell with PP significantly increases while remaining stable in the cell with AuPP. At the 1,000th cycle (2,000 h), the voltage hysteresis of the cell with PP has grown to about 120 mV, whereas in the

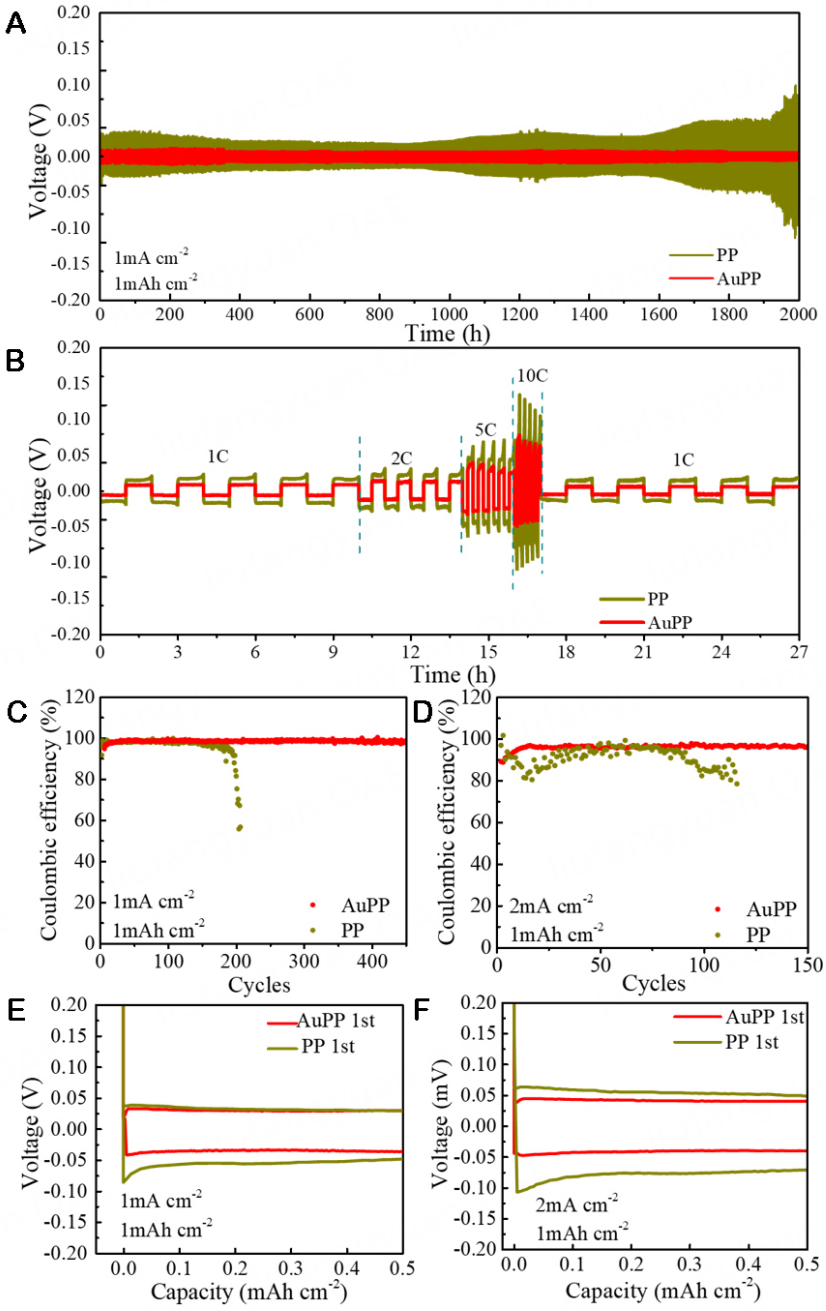

Figure 3. Electrochemical performance of cells with/without AuPP. (A) Voltage profiles for symmetrical Li|Li cells with PP and AuPP. (B) Rate performance of symmetrical Li cells with PP and AuPP. Coulombic efficiency of half-cells Li|Cu for 1 mA h cm^{-2} at (C) 1 mA cm^{-2} and (D) 2 mA cm^{-2}. (E) Voltage profile of the 1st cycle of half-cells Li|Cu with PP and AuPP for 1 mA h cm^{-2} at (E) 1 mA cm^{-2} and (F) 2 mA cm^{-2}.

cell with AuPP, it is just 4.7 mV. As shown in Figure 3B, when the current density increases from 1 to 10 C and then back to 1 C, the cell with AuPP exhibits a relatively more stable voltage hysteresis and smaller polarization voltage at large current densities than that of the cell with PP. These superior electrochemical performances come from the uniform nucleation and sequent uniform lithium deposition on AuPP. At the current density of 1 mA cm^{-2}, the half-cell Li|Cu with AuPP shows a long cycle life of 450 cycles and remains at a high CE of 98.62% [Figure 3C]. Reverse growth direction is an important reason for this long cycle life.

Meanwhile, the cell with PP only remains 150 cycles. After this, CE drops sharply, and eventually, the cell cannot work. When the current density increases to 2 mA cm^{-2}, both cycle lifespans decrease due to the much more severe lithium dendrite issue [Figure 3D]. The CE of the cell with AuPP stays at 96.01% after 150 cycles, while that of the cell with PP remains unstable and finally declines after 80 cycles. From Figure 3E and F, the cells with PP show much larger polarization voltage in the first cycle in two current densities, consistent with higher nucleation barrier discussed earlier. To verify the internal impedance and interfacial stability, electrochemical impedance spectroscopy (EIS) spectra of the cells after 100 cycles at a current density of 1 mA cm^{-2} and a surface capacity of 1 mA h cm^{-2} were tested [Supplementary Figure 8]. AuPP cells exhibit lower interfacial impedance because the good affinity of AuPP for lithium reduces the SEI growth and the "dead Li" generation, thus helping stabilize good electrode-electrolyte contact during repeated deposition/stripping.

The morphology evolution of deposited lithium after cycles at 1 mA cm^{-2} of 1 mA h cm^{-2} is evaluated, as shown in Figure 4. After one cycle, deposited lithium on AuPP [Figure 4A] remains flat and dense, and no lithium is deposited on the opposite Cu [Figure 4D]. This verifies that lithium prefers to plate on the AuPP rather than on the Cu. In contrast, deposited lithium of the cell with PP on Cu is uneven and of different sizes [Figure 4J] due to the lithiophobic trait of Cu and uneven lithium nucleation. No lithium deposit is on the opposite PP [Figure 4G]. After five and ten cycles, the lithium morphology significantly differs on AuPP [Figure 4B and C] and Cu [Figure 4K and L]. There are also massive residual SEIs on the underlying Cu, especially after ten cycles, which have consumed too much electrolyte and will lead to dead lithium from dendrites, causing short life and low CE for cells. These results demonstrate the mechanism discussed above of this design: Au lowers the nucleation barrier and provides uniform nucleation sites for lithium depositing, and lithium prefers to deposit on Au and grows to the Cu side.

To assess the feasibility for practically applying this modified AuPP, full cells using $LiFePO_4$ cathodes are tested. To better suit practical use, an amount of 1 mA h cm^{-2} lithium has been pre-deposited on AuPP or Cu at 1 mA cm^{-2} as the anode [Figure 5A]. They are the only lithium source in Li|$LiFePO_4$ full cells. The areal density of $LiFePO_4$ is 4.2 mg cm^{-2}. The N/P ratio is 1.40 in our design, while it ranges from 1.03 to 1.2 in commercial lithium-ion batteries. After 800 cycles, the cell with AuPP remains at a better capacity of 82.1 mA h g^{-1} and a higher CE of 99.23%. The capacity of the cell with PP decreases sharply after 550 cycles and reaches close to zero in the 700th cycle. As the cycles increase, the voltage hysteresis between discharge and charge plateaus of the cell with AuPP remains almost unchanged [Figure 5B]. However, the voltage hysteresis of the cell with PP displays a gradually expanding trend. When the current density increases from 0.5 to 5 C, the cell with AuPP exhibits higher capacities, and has a better recovery capacity from 5 to 0.5 C, manifesting the better charge transfer during cycling [Figure 5C]. The voltage hysteresis of the cell with AuPP keeps stable discharge and charge plateaus even at 5 C [Figure 5D]. In all, Li|$LiFePO_4$ full cells with AuPP display excellent application potential.

CONCLUSIONS

In summary, we achieved uniform lithium deposition and guided its growth in an opposite direction to normal with 13.4 nm Au-modified PP. Lithium prefers to deposit on Au rather than on Cu due to a higher binding energy (3.056 to 2.500 eV), leading to the opposite lithium growth direction. Furthermore, because of the nucleation barrier close to zero and lithiophilic feature, lithium nucleates on the Au layer and grows uniformly, which can alleviate the lithium dendrite growth. This designed AuPP helps improve the electrochemical performance of lithium metal anodes. With the AuPP, symmetric cells attain a long lifespan of 2,000 h with stable voltage hysteresis, and the half cell keeps a high CE of 98.62% after 450 cycles at 1 C, three times the cell without AuPP. The full cell exhibits an excellent life of 800 cycles at 1 C when paired

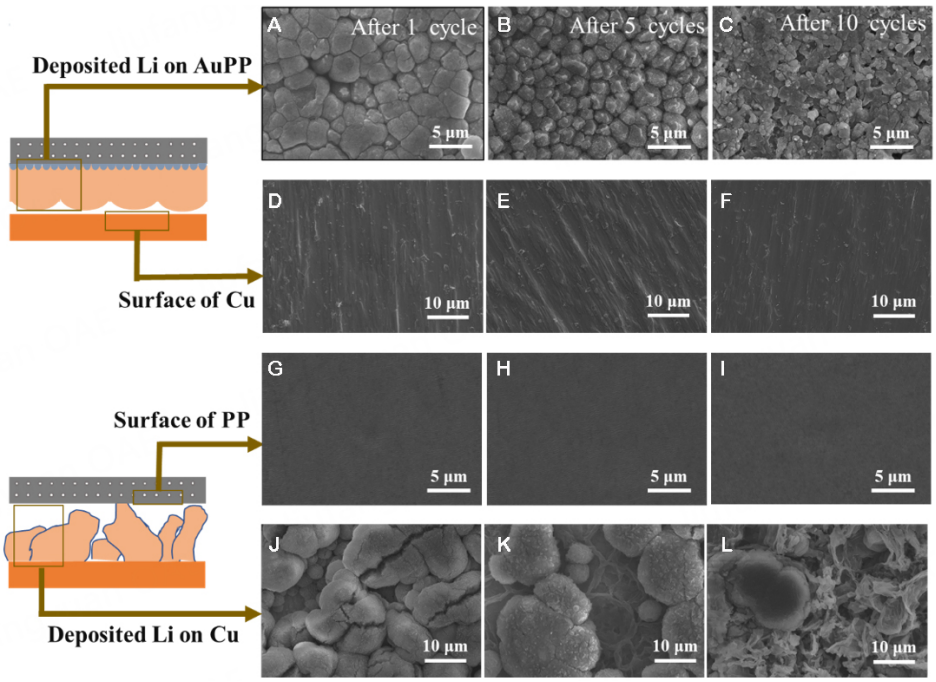

Figure 4. Top view of morphology of deposited lithium and Cu foil in the cells with AuPP and deposited lithium and separator in the cells without AuPP after cycles at 1 mA cm^{-2} for 1 mA h cm^{-2} after 1st, 5th and 10th cycles. (A-C) Deposited lithium on the AuPP. (D-F) Cu in cells with AuPP. (G-I) Separator in cells without AuPP. (J-L) Deposited lithium on Cu in cells without AuPP.

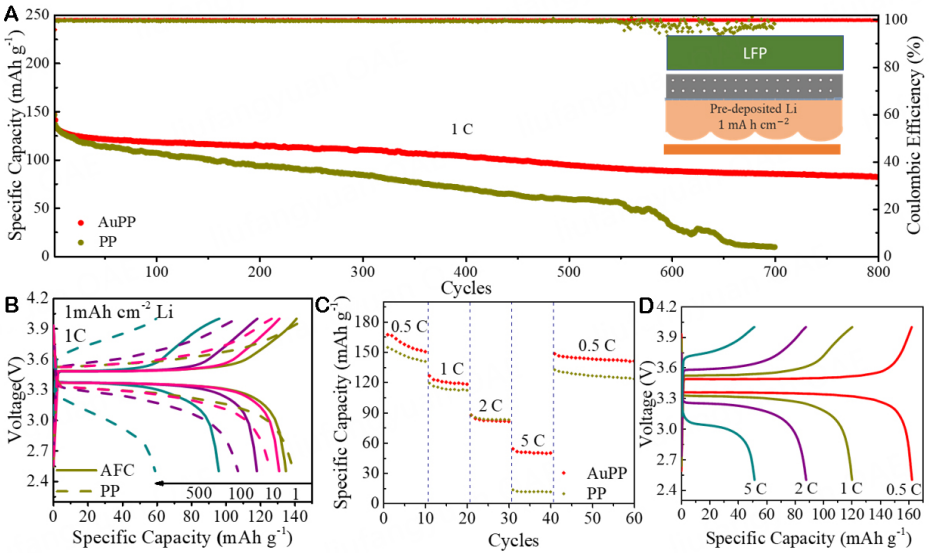

Figure 5. Electrochemical performance of Li|$LiFePO_4$ cells. (A) Cycle life of Li|$LiFePO_4$ with PP and AuPP at 1 C. The amount of 1 mA h cm^{-2} of lithium is pre-deposited on the AuPP and Cu, respectively. (B) Voltage profile of different cycles of Li|$LiFePO_4$ cells with and without Au modified-separators at 1 C. (C) Rate performance of cells with PP and AuPP at the current density of 0.5, 1, 2, 5 and 0.5 C. (D) Voltage profile of cells with AuPP at different current density.

with a $LiFePO_4$ cathode. In all, the preparation of AuPP can be easily scaled up, and this design achieves superior electrochemical performances for lithium metal anodes.

DECLARATIONS

Acknowledgments

SEM imaging was conducted at the Center for Advancing Materials Performance from the Nanoscale (CAMP NANO). We thank Dr. Chaowei Guo for his help with SEM. Han X acknowledges the Independent Research Project of the State Key Laboratory of Electrical Insulation and Power Equipment for financial support.

Authors' contributions

Manuscript writing: Sun Z
Manuscript revision: Shen F, Han X
Approved the final version of the manuscript: Sun Z, Zhang Q, Wang Z, Chen Y, Wang K, Shen F, Guo J, Han X

Availability of data and materials

The following files are available free of charge. Characterization data (PDF).

Financial support and sponsorship

This work was supported by the National Key R&D Program of China (Grant No. 2020YFA0710500), and the Key Research and Development Program of Shaanxi (Program No.2022GXLH-01-23).

Conflicts of interest

All authors declared that there are no conflicts of interest.

Ethical approval and consent to participate

Not applicable.

Consent for publication

Not applicable.

REFERENCES

1. Zou P, Wang Y, Chiang SW, Wang X, Kang F, Yang C. Directing lateral growth of lithium dendrites in micro-compartmented anode arrays for safe lithium metal batteries. *Nat Commun* 2018;9:464. DOI PubMed PMC
2. Shen F, Zhang F, Zheng Y, et al. Direct growth of 3D host on Cu foil for stable lithium metal anode. *Energy Storage Mater* 2018;13:323-8. DOI
3. Hou G, Sun Q, Ai Q, et al. Growth direction control of lithium dendrites in a heterogeneous lithiophilic host for ultra-safe lithium metal batteries. *J Power Sources* 2019;416:141-7. DOI
4. Wang H, Lin D, Xie J, et al. An interconnected channel-like framework as host for lithium metal composite anodes. *Adv Energy Mater* 2019;9:1802720. DOI
5. Cui C, Yang C, Eidson N, et al. A highly reversible, dendrite-free lithium metal anode enabled by a lithium-fluoride-enriched interphase. *Adv Mater* 2020;32:e1906427. DOI
6. Zhu B, Jin Y, Hu X, et al. Poly(dimethylsiloxane) thin film as a stable interfacial layer for high-performance lithium-metal battery anodes. *Adv Mater* 2017;29:1603755. DOI
7. Wang G, Chen C, Chen Y, et al. Self-stabilized and strongly adhesive supramolecular polymer protective layer enables ultrahigh-rate and large-capacity lithium-metal anode. *Angew Chem Int Ed* 2020;59:2055-60. DOI
8. Ma J, Quhe R, Zhang Z, et al. Two-dimensional materials as a stabilized interphase for the solid-state electrolyte $Li_{10}GeP_2S_{12}$ in lithium metal batteries. *J Mater Chem A* 2021;9:4810-21. DOI
9. Umh HN, Park J, Yeo J, Jung S, Nam I, Yi J. Lithium metal anode on a copper dendritic superstructure. *Electrochem Commun* 2019;99:27-31. DOI
10. Yi J, Chen J, Yang Z, et al. Facile patterning of laser-induced graphene with tailored Li nucleation kinetics for stable lithium-metal batteries. *Adv Energy Mater* 2019;9:1901796. DOI

11. Cao Z, Li B, Yang S. Dendrite-free lithium anodes with ultra-deep stripping and plating properties based on vertically oriented lithium-copper-lithium arrays. *Adv Mater* 2019;31:e1901310. DOI PubMed
12. Luo Y, Guo L, Xiao M, et al. Strategies for inhibiting anode dendrite growth in lithium-sulfur batteries. *J Mater Chem A* 2020;8:4629-46. DOI
13. Pu J, Li J, Shen Z, et al. Interlayer lithium plating in Au nanoparticles pillared reduced graphene oxide for lithium metal anodes. *Adv Funct Mater* 2018;28:1804133. DOI
14. Yang C, Yao Y, He S, Xie H, Hitz E, Hu L. Ultrafine silver nanoparticles for seeded lithium deposition toward stable lithium metal anode. *Adv Mater* 2017;29:1702714. DOI
15. Zhang Y, Luo W, Wang C, et al. High-capacity, low-tortuosity, and channel-guided lithium metal anode. *Proc Natl Acad Sci USA* 2017;114:3584-9. DOI PubMed PMC
16. Huang S, Zhang W, Ming H, Cao G, Fan LZ, Zhang H. Chemical energy release driven lithiophilic layer on 1 m^2 commercial brass mesh toward highly stable lithium metal batteries. *Nano Lett* 2019;19:1832-7. DOI
17. Pu J, Li J, Zhang K, et al. Conductivity and lithiophilicity gradients guide lithium deposition to mitigate short circuits. *Nat Commun* 2019;10:1896. DOI PubMed PMC
18. Zheng H, Zhang Q, Chen Q, et al. 3D lithiophilic-lithiophobic-lithiophilic dual-gradient porous skeleton for highly stable lithium metal anode. *J Mater Chem A* 2020;8:313-22. DOI
19. Tang L, Zhang R, Zhang X, et al. ZnO nanoconfined 3D porous carbon composite microspheres to stabilize lithium nucleation/growth for high-performance lithium metal anodes. *J Mater Chem A* 2019;7:19442-52. DOI
20. Wang X, Zeng W, Hong L, et al. Stress-driven lithium dendrite growth mechanism and dendrite mitigation by electroplating on soft substrates. *Nat Energy* 2018;3:227-35. DOI
21. Zhang D, Dai A, Fan B, et al. Three-dimensional ordered macro/mesoporous Cu/Zn as a lithiophilic current collector for dendrite-free lithium metal anode. *ACS Appl Mater Interfaces* 2020;12:31542-51. DOI
22. Qin L, Wang K, Xu H, et al. The role of mechanical pressure on dendritic surface toward stable lithium metal anode. *Nano Energy* 2020;77:105098. DOI
23. Liu X, Liu J, Qian T, Chen H, Yan C. Novel organophosphate-derived dual-layered interface enabling air-stable and dendrite-free lithium metal anode. *Adv Mater* 2020;32:e1902724. DOI
24. Lu Z, Li W, Long Y, et al. Constructing a high-strength solid electrolyte layer by in vivo alloying with aluminum for an ultrahigh-rate lithium metal anode. *Adv Funct Mater* 2020;30:1907343. DOI
25. Jeon H, Yeon D, Lee T, Park J, Ryou M, Lee YM. A water-based Al_2O_3 ceramic coating for polyethylene-based microporous separators for lithium-ion batteries. *J Power Sources* 2016;315:161-8. DOI
26. Cho J, Jung Y, Lee YS, Kim D. High performance separator coated with amino-functionalized SiO_2 particles for safety enhanced lithium-ion batteries. *J Membrane Sci* 2017;535:151-7. DOI
27. Mao X, Shi L, Zhang H, et al. Polyethylene separator activated by hybrid coating improving Li^+ ion transference number and ionic conductivity for Li-metal battery. *J Power Sources* 2017;342:816-24. DOI
28. Sabetzadeh N, Falamaki C, Riahifar R, et al. Plasma treatment of polypropylene membranes coated with zeolite/organic binder layers: assessment of separator performance in lithium-ion batteries. *Solid State Ion* 2021;363:115589. DOI
29. Liu M, Zhang P, Gou L, Hou Z, Huang B. Enhancement on the thermostability and wettability of lithium-ion batteries separator via surface chemical modification. *Mater Lett* 2017;208:98-101. DOI
30. Pan L, Wang H, Wu C, Liao C, Li L. Tannic-acid-coated polypropylene membrane as a separator for lithium-ion batteries. *ACS Appl Mater Interfaces* 2015;7:16003-10. DOI
31. Zhao Y, Yan J, Cai W, et al. Elastic and well-aligned ceramic LLZO nanofiber based electrolytes for solid-state lithium batteries. *Energy Storage Mater* 2019;23:306-13. DOI
32. Cao C, Li Y, Feng Y, Peng C, Li Z, Feng W. A solid-state single-ion polymer electrolyte with ultrahigh ionic conductivity for dendrite-free lithium metal batteries. *Energy Storage Mater* 2019;19:401-7. DOI
33. Han X, Gong Y, Fu KK, et al. Negating interfacial impedance in garnet-based solid-state Li metal batteries. *Nat Mater* 2017;16:572-9. DOI
34. Kresse G, Hafner J. Ab initio molecular dynamics for liquid metals. *Phys Rev B Condens Matter* 1993;47:558-61. DOI PubMed
35. Kresse G, Furthmüller J. Efficiency of ab-initio total energy calculations for metals and semiconductors using a plane-wave basis set. *Comp Mater Sci* 1996;6:15-50. DOI
36. Blöchl PE. Projector augmented-wave method. *Phys Rev B Condens Matter* 1994;50:17953-79. DOI PubMed
37. Perdew JP, Ruzsinszky A, Csonka GI, et al. Restoring the density-gradient expansion for exchange in solids and surfaces. *Phys Rev Lett* 2008;100:136406. DOI
38. Henkelman G, Uberuaga BP, Jónsson H. A climbing image nudged elastic band method for finding saddle points and minimum energy paths. *J Chem Phys* 2000;113:9901-4. DOI
39. Yan K, Lu Z, Lee H, et al. Selective deposition and stable encapsulation of lithium through heterogeneous seeded growth. *Nat Energy* 2016;1:16010. DOI